Wiesner, Maciej; Koski, Kristie; Laitinen, Antti; Manninen, Juuso; Zyuzin, Alexander A.; Hakonen, Pertti

Electron–phonon coupling in copper intercalated Bi_2Se_3

Published in:
Scientific Reports

DOI:
10.1038/s41598-022-15909-w

Published: 15/07/2022

Document Version
Publisher's PDF, also known as Version of record

scientific reports

Check for updates

OPEN

Electron–phonon coupling in copper intercalated Bi_2Se_3

Maciej Wiesner[1], Kristie Koski[2], Antti Laitinen[3,4], Juuso Manninen[3], Alexander A. Zyuzin[3] & Pertti Hakonen[3]✉

We report charge and heat transport studies in copper-intercalated topological insulator Bi_2Se_3 hybrid devices. Measured conductivity shows impact of quantum corrections, electron–electron and electron–phonon interactions. Our shot noise measurements reveal that heat flux displays a crossover between T^2 and T^4 with the increase of temperature. The results might be explained by a model of inelastic electron scattering on disorder, increasing the role of transverse acoustic phonons in the electron–phonon coupling process.

Charge and heat transport in metals are governed by the interplay between the electron scattering from impurities, quantum corrections, electron–electron (EE) and electron–phonon (EP) interactions. Here we study the temperature dependence of conductivity and heat flux in weakly copper-intercalated topological insulator (TI) Bi_2Se_3. Although, the quantum and EE corrections to the conductivity in Bi_2Se_3 have been extensively studied[1–7] and the strength of the electron–phonon coupling has been determined e.g. by using ARPES[8] and surface phonons[9], very little is known about the effect of the interference between EP and electron-impurity scattering on electrical transport, which has been of great interest in disordered metallic conductors[10] and nanowires[11].

This interference arises via impurities that move along with the phonons, i.e. via vibrating impurities. In disordered materials, for example intercalated crystals, the vibrating impurities due to the EP and electron-impurity interference result in a T^2 contribution to conductivity[12]. Besides intercalated atoms, also interstitial doping can lead to a T^2 contribution in the resistance[13], whereas in clean Bi_2Se_3 only very limited T^2 contribution is observed[14].

In general, the contribution of phonons to the low-temperature conductivity can be analysed by introducing two characteristic temperatures. First is the Bloch–Grüneisen temperature T_{BG}, which is associated with the particles' Fermi surface. Second is the temperature at which the phonon wave length becomes comparable to the mean free path of electrons due to scattering on impurities[12,15–17]. It can be estimated as $T_{dis} = 2\pi\hbar v_s/(k_B L_e)$, where v_s is the sound velocity, L_e the electron mean-free path, and $\hbar$, k_B are the Planck and Boltzmann constants, respectively. Note the sound velocities of longitudinal and transverse modes are different, which has to be taken into consideration in an analysis of the EP interaction and determination of characteristic temperatures in the material.

Coupling of electrons to longitudinal and transverse acoustic phonons is a complex problem, which has been widely analysed in clean systems $T_{dis} \ll T$[18]. In pure materials, electrons do not interact with transverse phonons in the lowest order in the EP interaction term. Fundamentally, for clean Bi_2Se_3, the phonon contribution to the resistance in the bulk is given by the Bloch–Grüneisen term $\propto T^5$ at low temperatures $T_{dis} << T < T_{BG}$[19], while $\propto T^4$ is expected for thin crystals[20].

In impure materials, however, electron interactions with transverse phonons contribute to the charge transport. In the case of all impurities moving with the phonon displacement field, the resistance at temperatures $T_{dis} \lesssim T \lesssim T_{BG}$ is given by[10,12]:

$$\frac{R - R_0}{R_0} = \left[1 - \frac{1}{2}\left(\frac{v_t}{v_\ell}\right)^3 \left(1 - \frac{\pi^2}{16}\right)\right] \frac{\beta_t}{v_t} \frac{(2\pi k_B T)^2}{3E_F p_F \hbar} \tag{1}$$

where R_0 is the resistance determined by the electron scattering on disorder, E_F is the chemical potential, p_F is the Fermi momentum, β_ℓ and β_t are the constants of interaction with longitudinal and transverse phonons with velocities v_ℓ and v_t, respectively. The interaction constants satisfy $\beta_t/\beta_\ell = (v_\ell/v_t)^2$ and can be retrieved from the experimental data. For Bi_2Se_3, taking into account $v_t = 1.7$ km/s and $v_\ell = 3.5$ km/s , $\beta_t/\beta_\ell \approx 4$ emphasises

[1]Faculty of Physics, Adam Mickiewicz University, Poznan, Poland. [2]Department of Chemistry, University of California Davis, Davis, CA, USA. [3]Low Temperature Laboratory, Department of Applied Physics, Aalto University, P.O. Box 15100, 00076 Aalto, Finland. [4]Department of Physics, Harvard University, Cambridge, MA 02138, USA. ✉email: pertti.hakonen@aalto.fi

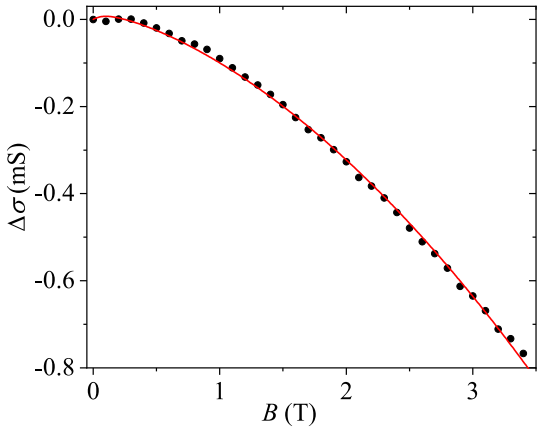

Figure 1. Magnetoconductivity $\Delta\sigma = \sigma(B,T) - \sigma(T)$ measured at $T = 100$ mK. The red curve is a fit obtained using Eq. (3) together with a small linear magnetoresistance component. The weak localisation in the bulk is described by $\alpha = 1$ and $L_\phi = 293$ nm. Other fit parameters are discussed in the text. At low magnetic fields the magnetoconductivity can be affected by effects related with Andreev reflection or proximity induced superconductivity due to aluminium contacts deposited on top surface of the TI.

stronger contribution of transverse than longitudinal phonons, quite similar to disordered metal samples in Ref.[10]. We note that the crossover between T^2 and T^5 laws in resistivity depends on the mean free path and the coefficients of electron interaction with transverse and longitudinal phonons[16].

The heat transport by electrons as opposed to relaxation by coupling to phonons can be distinguished in shot noise measurements. In particular, the heat flux between hot electrons and phonons with temperatures T_e and T_{ph}, respectively, scales as $P(T_e, T_{ph}) \propto T_e^k - T_{ph}^k$ (T_e will be defined in Methods section). The power law k is sensitive to the dimensionality of the sample[21], disorder[12,17,22], type of phonons[12], screening[23] and chirality[24] of charge carriers. Here we distinguish the heat flux mechanism, which is determined by the transverse phonons at $T_{dis} \lesssim T \lesssim T_{BG}$[16],

$$P\left(T_e, T_{ph}\right) = \frac{\pi^2 \beta_t}{10\hbar^3} \frac{V}{L_e \nu_F \nu_t} \left[(k_B T_e)^4 - (k_B T_{ph})^4\right], \tag{2}$$

where ν_F is the Fermi velocity and V is the volume of the sample.

In this paper we present experimental results for the temperature dependence of the conductivity and heat flux in the copper intercalated Bi_2Se_3. We focus on the signatures of electron–phonon interaction contribution to the observables. First we comment on a crossover between EE and EP interaction corrections to the conductivity. Then we analyze the contribution of the EP interaction to the heat flux.

Results and discussion

Conductivity. Measurements of magnetoconductivity were performed at temperature $T = 100$ mK and magnetic field ranging from 0 up to 3.5 T, as shown in Fig. 1. Fitting of the results was based on a modified Hikami–Larkin–Nagaoka approach[25–27]. Besides the quantum corrections, we employed both linear ($\propto B$) and quadratic ($\propto B^2$) magnetoresistance components. Quadratic terms arise either from classical magnetoresistance or spin-orbit scattering. The origin of the linear magnetoresistance (LMR) $\propto B$ is not apparent but, indeed, it has been observed in topological insulators such as Bi_2Se_3[28,29] and Bi_2Te_3[30].

The magnetoconductivity $\Delta\sigma = \sigma(B,T) - \sigma(T)$ for Bi_2Se_3 can be written in the form[26,27,31]:

$$\Delta\sigma = \frac{\alpha e^2}{2\pi^2\hbar}\left[\Psi\left(\frac{B_\phi}{B} + \frac{1}{2}\right) - \ln\left(\frac{B_\phi}{B}\right)\right] + \beta B^2 + \gamma B \tag{3}$$

where α denotes the strength and nature of quantum corrections and $B_\phi = \frac{\hbar}{4e} L_\phi^{-2}$ defines a characteristic field related to dephasing length L_ϕ. The term $\beta B^2 = -\sigma(T)\mu^2 B^2 - \frac{e^2}{24\pi^2\hbar}\left[\left(\frac{B}{B_{SO}+B_e}\right)^2 - \frac{3}{2}\left(\frac{B}{\frac{4}{3}B_{SO}+B_\phi}\right)^2\right]$ where the first term $-\sigma(T)\mu^2 B^2$ denotes the classical, mobility-μ-dependent magnetoresistance ($\mu^2 B^2 \ll 1$), while the latter terms are the quantum corrections specified using characteristics fields $B_{SO,e} = \frac{\hbar}{4e} L_{SO,e}^{-2}$ given by spin-orbit scattering length L_{SO} and the mean free path L_e, respectively.

In general, the parameter α is a measure of the relative strengths of the spin-orbit interaction, inter-valley scattering, magnetic scattering, and dephasing, as discussed in Ref.[32] for topological insulators, and their value may vary between $-1 \cdots +1$ (or even down to -2[27]). Using weak localization (WL) $\alpha = 1$, our fit displayed in Fig. 1 yields $L_\phi = 293 \pm 100$ nm for the dephasing length, while the linear and quadratic terms amount to $\gamma = -0.11\,\mathrm{mS/T}$ and $\beta = -41\,\mu\mathrm{S/T}^2$, respectively. The value obtained for bulk dephasing length L_ϕ is consistent

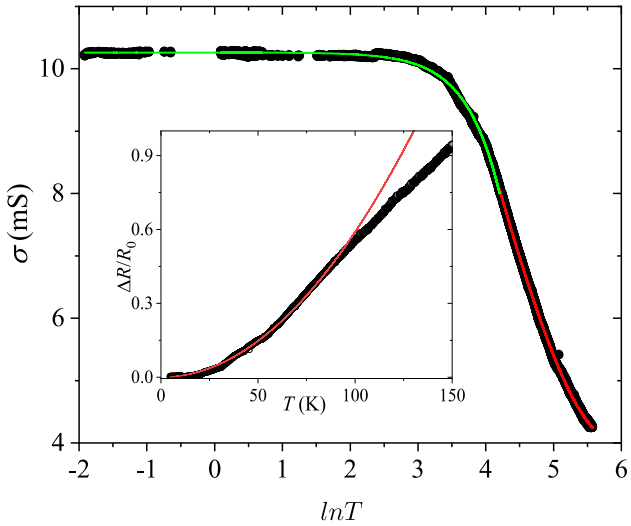

Figure 2. Temperature dependence of conductivity. The green line depicts a fit using Eq. (4), in which $\sigma_0 = 10$ mS, $k = 2$, $\alpha = 1$, and $d_2 \simeq -1 \times 10^{-6}$ S, while the red line illustrates linear resistivity at $T > T_{BG}$ The crossover temperature between the green and red curves is taken as the Bloch–Grüneisen temperature T_{BG}. An inset shows relative change in the sheet resistance. The red curve is a fit to the data with R_0 subtracted using Eq. (1): $(R - R_0)/R_0 = AT^2$, which gives for the prefactor $A = 59 \times 10^{-6}\,\mathrm{K}^{-2}$.

with the earlier result of 300 nm obtained in Cu-doped Bi_2Se_3[33]. We note that short dephasing length due to electron–electron scattering, would lead to the so-called hot electron regime, in which the noise power would increase linearly with temperature or bias voltage. This is clearly against our observations and electron–phonon scattering plays a role in the noise generation. Furthermore, the use of weak antilocalization theory with small L_ϕ is not able to reproduce the $\sigma(B)$ over the measured range of magnetic fields. In other words, the positive trend owing to weak localization corrections $dG/dB > 0$ is expected at magnetic fields $B \lesssim 30$ mT which is not discernible in Fig. 1.

The transport in our sample is nearly fully governed by the bulk contribution. In this situation, the term βB^2 turns out to be dominated by classical magnetoresistance $\Delta R \propto \mu^2 B^2$, because L_{SO} is expected to be much shorter than $L_\phi \simeq 300$ nm in the bulk[5] and $B_{SO} >> B_\phi$. Hence, we may identify $\beta = \sigma_0 \mu^2$ and obtain for the mobility of carriers $\mu = 0.0657$ m^2/Vs. Using $g = \sigma_0 \frac{\pi\hbar}{e^2}$, where $\sigma_0 = 9.5$ mS, we estimate the mean free path $L_e = g/k_F$=35 nm, where the Fermi momentum $k_F = 3.5 \times 10^9$ 1/m was obtained from the Bloch-Grüneisen temperature (see text related to Fig. 2). The mean free path $L_e = 35$ nm agrees directly with the one obtained from mobility $\mu = qL_e/2m_{\mathrm{eff}}v_F$, using an effective mass $m_{\mathrm{eff}}/m_0 = 0.11$ where m_0 is the free electron mass. This m_{eff} is close to the values obtained in Refs.[34,35]. Three principal remarks on the measured $\sigma(B)$ are in order. First, neglecting contribution of the surface states, the bulk WL behavior in $\sigma(B)$ suggests a situation of weakly doped topological insulator with the chemical potential close to the conduction band gap[31,32]. To describe the data, the model of parabolic bulk conduction band may be utilized to describe the properties of copper intercalated Bi_2Se_3 topological insulator. In this limit, one may expect similar temperature dependencies of conductivity and heat flux between hot electrons and phonons. Second, taking the bulk transverse and longitudinal phonon velocities we can estimate the characteristic temperatures at which thermal phonon wave-length becomes comparable to the electron mean free path. We estimate the $T_{\mathrm{dis}} = 2.3$ K and 4.8 K for transverse and longitudinal phonons, respectively. Third, at low temperature $T \simeq 100$ mK, the dephasing length $L_\phi \simeq 300$ nm is appreciably longer than $L_e \simeq 35$ nm, which implies several scattering events before the phase coherence is lost.

To proceed, the temperature dependence of conductivity was measured and the Bloch–Grüneisen temperature was identified as an inflection point on the R vs. T dependence at $T_{BG} = 90$ K.

We observe crossover between the logarithmic temperature dependence at low temperatures originating from competing interference and EE interaction corrections as well as T^2 behavior at higher temperatures, which we assign to the EP interaction processes. We note that estimated T_{dis} is slightly lower than the crossover temperature. The conductivity may be described by the formula:

$$\sigma = \sigma_0 + \frac{\alpha e^2}{2\pi^2\hbar}\ln(T/\mathrm{K}) + d_k(T/\mathrm{K})^k, \tag{4}$$

where α and d_k are parameters and K stands for Kelvin. At $T \lesssim 10$ K, the temperature dependence of conductivity is governed by the quantum interference and EE interaction corrections for a system with effective 2D diffusion, which is described by the second term in Eq. (4), having most commonly a positive sign due to the domination by EE interactions[31]. In the interval 10 K $\lesssim T < T_{BG}$, we observe signatures of the interference between the EP and electron-impurity scatterings Ref.[12]. This mechanism is described by the third term in Eq. (4), with $k = 2$. For surface states, the electron–phonon coupling has been found to display linear temperature dependence in

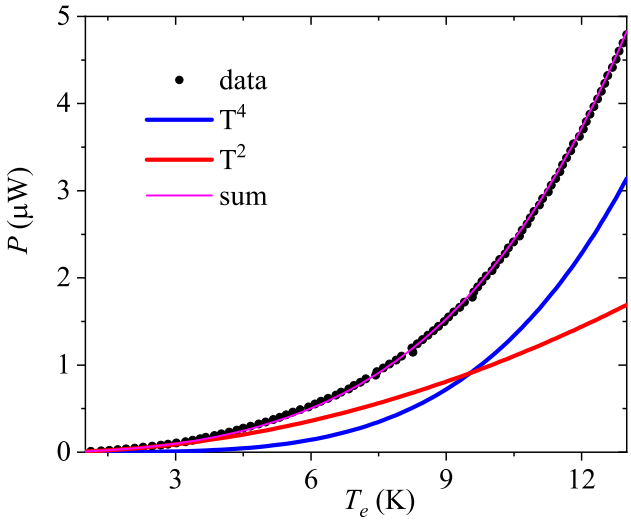

Figure 3. Joule heating power $P = IV$ as a function of temperature T_e deduced from the measured shot noise. The power is fitted using $P(T_e) = c_2 T_e^2 + c_4 T_e^4$ (magenta trace), which is a sum of electronic heat diffusion to the leads (red trace) and $P(T_e, T_{ph} = 0) \propto T_e^4$ given in Eq. (2) (blue trace). The red and blue traces correspond to parameters $c_2 = 1.0 \times 10^{-8}\,\mu\mathrm{WK}^{-2}$ and $c_4 = 1.1 \times 10^{-10}\,\mu\mathrm{WK}^{-4}$, respectively. A crossover from electronic heat diffusion towards electron–phonon coupling dominated heat transfer is observed at $T = 9.4$ K. Measurements were made at the phonon bath temperature of 50 mK.

resistance[36]. Under large bias, coupling to optical phonons with exponential activation behavior has also been observed[37].

Equivalently, one can rewrite the last term in Eq. (4) as a correction to the resistance as is done in Eq. (1). There the ratio of v_ℓ/v_t determines the sign of the correction. Noting $\frac{1}{2}(v_t/v_\ell)^3\left(1-\pi^2/16\right) \approx 0.02$ suggests that the dominant contribution to the EP interaction is due to transverse phonons in the investigated temperature range.

To find the EP interaction constants, one can rewrite Eq. (1) as $(R - R_0)/R_0 = AT^2$. The prefactor $A = 59 \times 10^{-6}\ \mathrm{K}^{-2}$ is obtained by fitting the quadratic behavior to the experimental data in Fig. 2. According to theory[10], the parameter A does not depend on the amount of impurities but on the ratio of dynamic impurities to static ones. Because precise control of Cu intercalation in the TI is hard to achieve at low levels, we decided to study only samples with an average Cu intercalation of 0.02%. Across the studied samples, the obtained values for A remained constant within a factor of 2. The Fermi momentum can be estimated as $k_F = k_B T_{BG}/2\hbar v_t \approx 3.5\,\mathrm{nm}^{-1}$, which allows us to estimate the chemical potential $E_F = v_F \hbar k_F/2 \approx (0.46 \pm 0.11)$ eV for typical Fermi velocity $v_F = (4 \pm 1) \times 10^5$ m/s in Bi_2Se_3. Please note that the chemical potential is measured with respect to the bottom of the conduction band. We find the EP interaction factors $\beta_t = 1.07 \pm 0.26$ and $\beta_\ell = \beta_t (v_t/v_\ell)^2 = 0.27 \pm 0.07$.

Heat flux between electrons and phonons. At low temperatures, due to the depopulation of phonon modes and the degeneracy of the electron system, the two subsystems of a normal metal, the electrons and the phonons, become almost isolated from each other. For this reason, they can 'equilibrate' independently, that is, they may reach equilibrium distributions over the quasiparticle states at some effective temperatures that we shall denote by T_e (for electrons) and T_{ph} (for phonons). Here we consider the so called "hot electrons" regime $T_e \gg T_{ph}$. In the hot electron regime, electrons in Bi_2Se_3 have such a large energy that they can transfer heat by diffusion to the aluminum measurement leads effectively. Consequently, electronic thermal conductance in the Al lead dominates over heat transfer to phonons at bias voltages on the order of 1–2 mV[38].

The temperature dependence of the heat flow $P(T)$ out from electrons in Bi_2Se_3 displays both T^2 and T^4 dependencies as seen in Fig. 3, which depicts Joule heating $P = IV$ vs. T_e determined from the measured non-equilibrium noise. At temperatures $T_e < 9$ K, electrons are the main heat carriers, which is reflected in the observed dependence $P \propto T_e^2$. Assuming homogeneous structure of investigated samples an analysis of the power dissipation at $T_e > 9$ K can be performed taking $P \propto T_e^4$ (Fig. 3). If we were to fit a higher order polynomial to the data, the terms for T^3 behavior would be on the 1%-2% level. Hence, the decomposition of the heat flow to T^2 and T^4 is accurate, but the uncertainty in the effective volume introduces an error on the order of ± (30–40)% in the electron–phonon coupling per unit volume. In the T^4 case one can relate the energy dissipation with contribution of dynamic scattering potential to the electron interaction with transverse phonons as has been analysed in Refs.[15,16]. A combined fit $P(T_e) = c_2 T_e^2 + c_4 T_e^4$ yields a perfect match to the data using parameters given in the caption of Fig. 3.

A T^4 temperature dependence could also arise for a heat flow limited by thermal boundary resistance in 3D systems (Kapitza resistance). It would reflect acoustic impedance mismatch of phonons across the interfaces made of Bi_2Se_3 and a SiO_2 substrate, as well as Bi_2Se_3 and metallic leads. This heat flow, $P(T_{ph}, T_0) = \frac{S}{4} A_K (T_{ph}^k - T_0^k)$, typically displays a Kapitza conductance of $A_K = 300 \ldots 500\ \mathrm{Wm}^{-2}\mathrm{K}^{-4}$ between metals and dielectric material[39–41]; here T_0 denotes the substrate phonon temperature. Using the contact area of the whole Bi_2Se_3

crystal to the SiO_2 substrate ($S_{SiO_2} = 4\,\mu m^2$) and the Al leads ($S_{Al} = 3\,\mu m^2$), we find that the Kapitza resistance cannot form a bottle neck in the thermal transport out from the sample.

An estimate for the strength of the interference contribution of the transverse phonons and random-scattering potential to the heat flux can be obtained from Eq. (2) in the limit $T_{ph} = 0$ K. By using $\beta_t = 1.07$, $v_F = 4 \times 10^5$ m/s, $L_e = 35$ nm, $v_t = 1.7$ km/s, and taking the volume of the sample as $V = 0.6 \times 10^{-13}$ cm^3, Eq. (2) evaluated at $T_e = 12$ K yields for the heat flow $P(T_e, 0) = 1.7\,\mu$W, which is in pretty good agreement with the heat flow given by the T^4 component extracted from the experimental data in Fig. 3. Note that there is no explicit dependence of $P(T_e, 0)$ on the Fermi velocity. However, if we identify T_{BG} as 100 K, $P(12\,K, 0) = 2.2\,\mu$W, nearly matching the measured power.

Discussion and conclusions

Typically, charge and heat transport in disordered materials is considered as an effect of electron scattering from the static and vibrating potentials, taking into account that the vibrating potential is completely dragged by phonons. A tacit assumption is made about averaged velocity of the phonons in the investigated system. In many materials, including layered topological insulators, such assumption is invalid. Velocities of transverse and longitudinal phonons differ significantly. Measurements of charge transport at low temperatures provide clear distinction of the effect of scattering on transverse and longitudinal phonons. According to Sergeev and Mitin[16] scattering of electrons on longitudinal phonons dominates in clean materials. Dynamic disorder, however, enhances electron coupling to transverse phonons.

Our studies of the transport properties of copper-intercalated Bi_2Se_3 indicate that intercalation may provide a tool for modification of the charge and heat transport in a topological insulator. The first influence of intercalation is slight enhancement of linear magnetoresistance at low fields $B < 2.5$T. Similar to the work of Ref.[28], the observed LMR could be related to electronic inhomogeneity, enhanced by intercalation in our work. We believe that the intercalated amount $x = 0.02\%$ is too small to validate the use of the disorder-induced LMR model of Parish and Littlewood in our samples[42].

At temperatures $T \lesssim 10$ K, the quantum and EE interaction corrections dominate the conductivity and the electronic heat flux, yielding $\sigma \propto \ln(T)$ and $P \propto T^2$, respectively. We emphasize that T_{dis} in principle does not coincide with the crossover temperature between the electron–phonon and electron–electron mechanism contributions to the electric conductivity. Here, we estimate T_{dis} to be lower than the crossover temperature between T^2 and T^4 behaviors. At $10\,K \lesssim T \lesssim T_{BG}$, the electron-transverse phonon interaction results in a T^2 temperature dependence of the conductivity, while the electron–phonon heat flux becomes $P \propto T^4$. The T^4 dependence for heat flux is predicted also for clean 2D conductors[17], and it has recently been observed e.g. in epigraphene[43]. In our case, however, the combination of T^2 dependent resistivity and T^4 dependent heat flow point strongly towards a disordered system with electron–phonon-impurity interference phenomena, which arise from vibrating impurities.

Methods

Single crystals of Bi_2Se_3 were grown using the vapour–liquid–solid (VLS) method and intercalated with zero-valent copper atoms using wet chemical intercalation[44]. It was assumed that copper intercalation in Bi_2Se_3 introduces disorder, which affects charge transport by enhanced scattering in the TI. Disorder in TIs can be introduced as doping (e.g. substitution of Bi atoms, which is called a compositional disorder) or as intercalation of van der Waals gaps (e.g. by zero-valent atoms as Cu, which is a structural disorder). Large intercalation rate takes place not only the van der Waals gaps but also in the interstitial sites of each layer, or it may exist as biatomic or triatomic layers in the van der Waals gaps[45]. This results in structural deformation, particularly in z-direction ($0.12\% < x < 0.2\%$) with Cu atoms results in superconductivity of the TI[44]. Low intercalation ($x < 0.1\%$) doesn't affect the crystallographic structure of the TI and is a subject of our interest as a tool for modification of band structure of the TI.

The intercalation ratio $x = 0.02\%$ was determined from the energy-dispersive X-ray spectroscopy (EDX). Sound velocity, in plane, was investigated using the 90-degree equal-angle scattering geometry of the Brillouin light spectroscopy (BLS) with a five pass scanning tandem Fabry–Pérot interferometer at $\lambda = 532$ nm. Results of the BLS experiments revealed transverse phonon velocity of 1700 m/s and longitudinal phonon velocity of 3500 m/s (Fig. 4).

We investigated hybrid devices made of Bi_2Se_3 topological insulator on SiO_2/Si substrate. We concentrated on representative data obtained for a sample with total dimensions Thickness × Width × Length = 60 nm × 1560 nm × 2500 nm, intercalated with 0.02% of Cu. A central section of length $L = 650$ nm and width $W = 1560$ nm was contacted using titanium/aluminium electrodes (5/45 nm). The resistance of the sample was 41 Ω at 4 K.

Our conductivity and current fluctuation experiments were performed on two pulse-tube-based dilution refrigerators operated around 0.015 K and 0.05 K. For experimental details, we refer to Refs.[46,47]. To determine the EP interaction and its effect on heat transport in our hybrid device, we deduce the non-equilibrium electronic temperature from shot noise measurements[48–50]. The Fano factor F is defined as the ratio of the measured noise level S_I and the Poissonian noise S_P, $F = S_I/S_P$. For diffusive electron transport the electronic temperature T_e is linearly dependent on F and the bias voltage V, $T_e = FeV/2k_B$[48]. Equivalently, we can use a calibration constant $\mathcal{M}$ to obtain the electronic temperature of the investigated system, $T_e = \mathcal{M}S(I)$. The constant was obtained as the ratio of the difference of the shot noise ΔS measured across two temperatures $T_1 = 900$ mK and $T_2 = 20$ mK: $\mathcal{M} = (T_2 - T_1)/\Delta S$. As defined in this manner, T_e denotes a spatial average over the temperature distribution in the Joule heated regime where EP scattering is investigated.

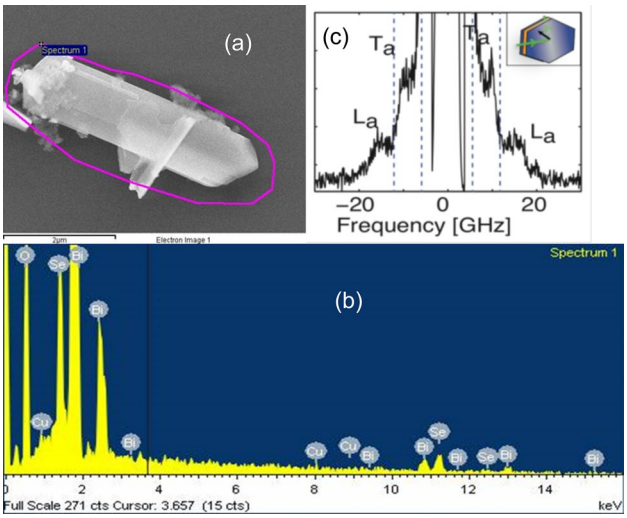

Figure 4. (**a**) SEM picture of a single crystal of intercalated Bi_2Se_3. (**b**) A result of the energy-dispersive X-ray spectroscopy showing 0.02% weight Cu intercalation of the TI. (**c**) The Brillouin Light Scattering spectrum of the Cu intercalated Bi_2Se_3 (Ta-transversal phonon La-longitudinal phonon).

Data availability

The datasets used and/or analysed during the current study are available at https://doi.org/10.5281/zenodo.6642016.

Received: 22 March 2022; Accepted: 30 June 2022
Published online: 15 July 2022

References

1. Checkelsky, J. G. *et al.* Quantum interference in macroscopic crystals of nonmetallic Bi_2Se_3. *Phys. Rev. Lett.* **103**, 246601 (2009).
2. Checkelsky, J. G., Hor, Y. S., Cava, R. J. & Ong, N. P. Bulk band gap and surface state conduction observed in voltage-tuned crystals of the topological insulator Bi_2Se_3. *Phys. Rev. Lett.* **106**, 196801 (2011).
3. He, H.-T. *et al.* Impurity effect on weak antilocalization in the topological insulator Bi_2Te_3. *Phys. Rev. Lett.* **106**, 166805 (2011).
4. Liu, M. *et al.* Crossover between weak antilocalization and weak localization in a magnetically doped topological insulator. *Phys. Rev. Lett.* **108**, 036805 (2012).
5. Steinberg, H., Laloë, J. B., Fatemi, V., Moodera, J. S. & Jarillo-Herrero, P. Electrically tunable surface-to-bulk coherent coupling in topological insulator thin films. *Phys. Rev. B.* **84**, 233101 (2011) arXiv:1104.1404.
6. Zhang, Y. *et al.* Crossover of the three-dimensional topological insulator Bi_2Se_3 to the two-dimensional limit. *Nat. Phys.* **6**, 584–588 (2010).
7. Stephen, G. M. *et al.* Weak antilocalization and anisotropic magnetoresistance as a probe of surface states in topological $Bi_2Te_xSe_{3-x}$ thin films. *Sci. Rep.* **10**, 4845 (2020).
8. Pan, Z.-H. *et al.* Measurement of an exceptionally weak electron–phonon coupling on the surface of the topological insulator Bi_2Se_3 using angle-resolved photoemission spectra. *Phys. Rev. Lett.* **108**, 187001 (2012) arXiv:1109.3638.
9. Zhu, X. *et al.* Electron–phonon coupling on the surface of the topological insulator Bi_2Se_3 determined from surface–phonon dispersion measurements. *Phys. Rev. Lett.* **108**, 185501 (2012) arXiv:1201.6346.
10. Ptitsina, N. *et al.* Electron–phonon interaction in disordered metal films: The resistivity and electron dephasing rate. *Phys. Rev. B.* **56**, 10089 (1997).
11. Hsu, W.-C. *et al.* Metallic conduction and large electron–phonon-impurity interference effect in single TiSi nanowires. *Nanosc. Res. Lett.* **7**, 500 (2012).
12. Reizer, M. Y. & Sergeev, A. V. The effect of the electron–phonon interaction of the conductivity of impure metals. *JETP* **65**, 1291 (1987).
13. Wang, J. *et al.* Evidence for electron–electron interaction in topological insulator thin films. *Phys. Rev. B* **83**, 245438 (2011) arXiv:1012.0271.
14. Mo, D. L., Wang, W. B. & Cai, Q. Influence of thickness on the electrical transport properties of exfoliated Bi_2Se_3 ultrathin films. *Nanosc. Res. Lett.* **11**, 354 (2016).
15. Reizer, M. Y. & Sergeev, A. V. Electron–phonon interaction in impure metals and superconductors. *JETP* **63**, 616 (1986).
16. Sergeev, A. & Mitin, V. Electron–phonon interaction in disordered conductors: Static and vibrating scattering potentials. *Phys. Rev. B.* **61**, 6041 (2000).
17. Chen, W. & Clerk, A. A. Electron–phonon mediated heat flow in disordered graphene. *Phys. Rev. B.* **86**, 125443 (2012).
18. Mahan, G. D. *Many-Particle Physics* 2nd edn. (Springer, 1990).
19. Giraud, S. & Egger, R. Electron–phonon scattering in topological insulators. *Phys. Rev. B* **83**, 245322 (2011).
20. Giraud, S., Kundu, A. & Egger, R. Electron–phonon scattering in topological insulator thin films. *Phys. Rev. B* **85**, 035441 (2012) arXiv:1111.4063..
21. Anghel, D. V., Caraiani, C. & Galperin, Y. M. Crossover temperature in electron–phonon heat exchange in layered nanostructures. *Phys. Scr.* **94**, 105704 (2019).
22. Xu, Z. Heat transport in low-dimensional materials: A review and perspective. *Theor. Appl. Mech. Lett.* **6**, 113–121 (2016).
23. Kubakaddi, S. S. Electron–phonon interaction in a quantum wire in the Bloch–Gruneisen regime. *Phys. Rev. B.* **75**, 075309 (2007).
24. Ansari, M. & Ashraf, S. S. Z. Chirality effect on electron phonon relaxation, energy loss, and thermopower in single and bilayer graphene in BG regime. *J. Appl. Phys.* **122**, 164302 (2017).

25. Hikami, S., Larkin, A. I. & Nagaoka, Y. Spin–orbit interaction and magnetoresistance in the two dimensional random system. *Prog. Theor. Phys* **63**, 707–710 (1980).
26. Hai Zhou, L., Shi, J. & Shen, S. Q. Competition between weak localization and antilocalization in topological surface states. *Phys. Rev. Lett.* **107**, 076801 (2011) arXiv:1101.5437.
27. Sasmal, S., Mukherjee, J., Suri, D. & Raman, K. V. In-depth analysis of anisotropic magnetoconductance in Bi_2Se_3 thin films with electron–electron interaction corrections. *J. Phys. Condens. Matter* **33**, 465601 (2021) arXiv:2106.07698.
28. Tang, H., Liang, D., Qiu, R. L. & Gao, X. P. Two-dimensional transport-induced linear magneto-resistance in topological insulator bi_2se_3 nanoribbons. *ACS Nano* **5**, 7510–7516 (2011).
29. Zhang, G. *et al.* Growth of topological insulator Bi_2Se_3 thin films on $SrTiO_3$ with large tunability in chemical potential. *Adv. Funct. Mater.* **21**, 2351–2355 (2011).
30. Qu, D. X., Hor, Y. S., Xiong, J., Cava, R. J. & Ong, N. P. Quantum oscillations and hall anomaly of surface states in the topological insulator Bi_2Te_3". *Science* **329**, 821–824 (2010).
31. Lu, H. Z. & Shen, S. Q. Weak localization and weak anti-localization in topological insulators. In *Spintron. VII*, Vol. 9167, Edited by Henri-Jean Drouhin, Jean-Eric Wegrowe, and Manijeh Razeghi (SPIE, 2014) p. 91672E.
32. Garate, I. & Glazman, L. Weak localization and antilocalization in topological insulator thin films with coherent bulk-surface coupling. *Phys. Rev. B.* **86**, 035422 (2012) arXiv:1206.1239.
33. Takagaki, Y., Jenichen, B., Jahn, U., Ramsteiner, M. & Friedland, K.-J. Weak antilocalization and electron-electron interaction effects in Cu-doped Bi_2Se_3 films. *Phys. Rev. B* **85**, 115314 (2012).
34. Butch, N. P. *et al.* Strong surface scattering in ultrahigh-mobility bi_2 se_3 topological insulator crystals. *Phys. Rev. B* **81**, 241301 (2010).
35. Brahlek, M., Koirala, N., Bansal, N. & Seongshik, O. Transport properties of topological insulators: Band bending, bulk metal-to-insulator transition, and weak anti-localization. *Sol. State Commun.* **215–216**, 54–62 (2015).
36. Kim, D. *et al.* Intrinsic electron–phonon resistivity of Bi_2Se_3 in the topological regime. *Phys. Rev. Lett.* **109**, 166801 (2012) arXiv:1205.5554..
37. Costache, M. V. *et al.* Fingerprints of inelastic transport at the surface of the topological insulator Bi_2Se_3. *Phys. Rev. Lett.* **112**, 086601 (2014) arXiv:1404.2198.
38. Voutilainen, J. *et al.* Energy relaxation in graphene and its measurement with supercurrent. *Phys. Rev. B* **84**, 045419 (2011).
39. Roukes, M. L., Freeman, M. R., Germain, R. S., Richardson, R. C. & Ketchen, M. B. Hot electrons and energy transport in metals at millikelvin temperatures. *Phys. Rev. Lett.* **55**, 422–425 (1985).
40. Swartz, E. T. & Pohl, R. O. Thermal boundary resistance. *Rev. Mod. Phys.* **61**, 605–668 (1989).
41. Elo, T. *et al.* Thermal relaxation in titanium nanowires: Signatures of inelastic electron-boundary scattering in heat transfer. *J. Low Temp. Phys.* **189**, 204–216 (2017) arXiv:1612.09424.
42. Parish, M. M. & Littlewood, P. B. Non-saturating magnetoresistance in heavily disordered semiconductors. *Nature* **426**, 162–165 (2003).
43. Karimi, B. *et al.* Electron–phonon coupling of epigraphene at millikelvin temperatures measured by quantum transport thermometry. *Appl. Phys. Lett.* **118**, 103102. https://doi.org/10.1063/5.0031315 (2021).
44. Koski, K. J. *et al.* Chemical intercalation of zerovalent metals into 2D layered Bi_2Se_3 nanoribbons. *J. Am. Chem. Soc.* **134**, 13773–13779 (2012).
45. López, P. A., Leal, F. M. & Derat, R. E. Structural and electronic characterization of $cu_xbi_2se_3$. *J. Mex. Chem. Soc* **60**, 101–107 (2016).
46. Danneau, R. *et al.* Evanescent wave transport and shot noise in graphene: Ballistic regime and effect of disorder. *J. Low Temp. Phys.* **153**, 374 (2008) arXiv:0807.0157.
47. Oksanen, M. *et al.* Single-mode and multimode Fabry-Pérot interference in suspended graphene. *Phys. Rev. B.* **89**, 121414 (2014).
48. Wu, F., Virtanen, P., Andresen, S., Plaçais, B. & Hakonen, P. J. Electron–phonon coupling in single-walled carbon nanotubes determined by shot noise. *Appl. Phys. Lett.* **97**, 262115 (2010).
49. Betz, A. C. *et al.* Supercollision cooling in undoped graphene. *Nat. Phys.* **9**, 109–112 (2013) arXiv:1210.6894.
50. Laitinen, A. *et al.* Electron–phonon coupling in suspended graphene: Supercollisions by ripples. *Nano Lett.* **14**, 3009–3013 (2014) arXiv:1510.09176.

Acknowledgements

This work was supported by Aalto University AScI Grant and the Academy of Finland projects 310086 (LTnoise) and 336813 (CoE Quantum Technology Finland). The research leading to these results has received funding from the European Union's Horizon 2020 Research and Innovation Programme, under Grant Agreement No. 824109. The work was partially sponsored by Polish National Centre of Science (NCN) grant 2015/17/B/ST3/02391. The work of AZ was supported by the Academy of Finland Grant No. 308339. AZ is grateful to the hospitality of the Pirinem School of Theoretical Physics.

Author contributions

M.W., A.L., J.M., P.H. performed the measurements. M.W. and A.L. analyzed the data. A.Z. and P.H. developed the theoretical model for the experimental findings. K.K. provided copper-intercalated Bi_2Se_3 single crystals. All authors contributed to preparation of the manuscript.

Competing interests

The authors declare no competing interests.

Additional information

Supplementary Information The online version contains supplementary material available at https://doi.org/10.1038/s41598-022-15909-w.

Correspondence and requests for materials should be addressed to P.H.

Reprints and permissions information is available at www.nature.com/reprints.

Publisher's note Springer Nature remains neutral with regard to jurisdictional claims in published maps and institutional affiliations.